1 **Technical note: Towards a stronger observational support for haze pollution control by**
2 **interpreting carbonaceous aerosol results derived from different measurement approaches**

3 Yuan Cheng, Ying-jie Zhong, Zhi-qing Zhang, Xu-bing Cao, Jiu-meng Liu[*]

4 State Key Laboratory of Urban Water Resource and Environment, School of Environment, Harbin
5 Institute of Technology, Harbin, 150090, China

6 [*] Corresponding author. Jiu-meng Liu (jiumengliu@hit.edu.cn).

7 **Abstract**

8 As China's fine particulate matter ($PM_{2.5}$) has decreased nationwide during the last decade, further

9 improvement of air quality became more challenging, imposing higher requirements on the

10 observational support for the understanding of aerosol sources. This was particularly the case for

11 the severe cold climate region in Northeast China, which suffered from relatively slow decreasing

12 rate and high exposure risk of $PM_{2.5}$. Here we evaluated carbonaceous aerosol data measured by

13 different sampling and analytical approaches, based on field campaigns conducted during a frigid

14 winter and an agricultural-fire impacted spring in Harbin. For both the high- and low-volume

15 sampling, a total of four sets of organic and elemental carbon results were derived by applying two

16 commonly-used temperature protocols (IMPROVE-A, i.e., IMPV, and NIOSH) to both untreated

17 filters and those extracted by methanol. Only the IMPV-based results measured before the extraction

18 were found to be indicative of aerosol sources, e.g., in reasonable accordance with secondary aerosol

19 formation in winter and open burning impacts in spring. Thus the analytical method of IMPROVE-

20 A on untreated samples was recommended for future field observations and source apportionments

21 of $PM_{2.5}$ in the studied region. In addition, although the low- and high-volume samplers typically

22 led to comparable measurement results for various species, exceptions were identified for water-

23 soluble potassium (K^+) and some fire-emitted chromophores. We suggested that K+ and light

24   absorption coefficients of brown carbon should be compared or integrated with caution across

25   studies using different PM$_{2.5}$ samplers.

1. Introduction

Carbonaceous aerosols are a complex mixture of compounds exhibiting a gradual change in chemical and physical properties (Pöschl, 2005; Andreae and Gelencsér, 2006), e.g., from colorless organics with low molecular weights, to "dark" brown carbon with relatively high thermal stabilities (Chakrabarty et al., 2023), and finally to refractory black carbon which is strongly light-absorbing. As important contributors to both fine particulate matter ($PM_{2.5}$) pollution and radiative forcing, they have long been targeted to achieve a synergistic improvement of air quality and mitigation of climate change (Fuzzi et al., 2015; von Schneidemesser et al., 2015; Liu et al., 2022). However, it remains a challenge to properly represent carbonaceous aerosols in chemical transport models, as each step along the way between the estimations of sources and tempo-spatial variations is difficult. For example, considerable uncertainties exist in the open burning emission, secondary organic aerosol (SOA) budget and black carbon lifetime (Andela et al., 2022; Chang et al., 2022; Zhong et al., 2023). This in turn introduces substantial uncertainties to the climate and health effects of carbonaceous aerosols (Li et al., 2022).

Field observational data on carbonaceous aerosols, including those derived from ground and aircraft measurements, are essential to constrain the simulation results and subsequently to improve the model performance (Philip et al., 2014; Wang et al., 2014b, 2018; Gao et al., 2022; Eckhardt et al., 2023). Relying on on-line instruments such as the Single Particle Soot Photometer (SP2), aircraft studies typically covered relatively short periods (e.g., up to about one month) but provided measurement results with high time and spatial resolutions (Samset et al., 2014). Offline and semi-continuous techniques (e.g., lab and field carbon analyzers for elemental carbon) were more commonly used in ground observations, producing datasets with relatively low time resolutions but

48   spanning several months to decades (Dao et al., 2019; Hand et al., 2024). After accounting for the

49   difference in time resolution, the integration of carbonaceous aerosol data across studies and regions

50   was still not straightforward. A major obstacle was caused by the multitude of measurement

51   principles (Petzold et al., 2013), which was intensively reflected by the considerable and, more

52   importantly, variable discrepancies in black carbon results among different methods (Buffaloe et al.,

53   2014; Li et al., 2019; Pileci et al., 2021; Tinorua et al., 2024). This problem was far from being

54   properly addressed, although great efforts have been devoted to refine the respective measurement

55   approach such as the thermal-optical (Cavalli et al., 2010), optical (Collaud Coen et al., 2010) and

56   SP2 (Laborde et al., 2012) techniques. In addition, this problem was to some extent overlooked in

57   China, which might be partially responsible for the inconsistent source apportionment results

58   obtained by different studies. For example, both Zheng et al. (2015) and Liu et al. (2020) applied

59   the elemental carbon (EC) tracer method to estimate secondary OC (SOC) during winter in Beijing,

60   but the two studies derived conflicted conclusions on the contribution of heterogeneous chemistry

61   to SOC formation (i.e., minimal vs. significant) since different analytical methods (i.e., NIOSH vs.

62   IMPROVE-A temperature protocols) for EC were deployed. Such inconsistencies substantially

63   weakened the observational support for the understanding of aerosol sources and thus the control of

64   haze pollution.

65   With a considerable decrease in the national $PM_{2.5}$ since 2013, it became more challenging to

66   further improve the air quality in China (Cheng et al., 2021). This imposed higher requirements on

67   the observational insights into aerosol sources, including the evaluation of carbonaceous aerosol

68   results among various measurement approaches. Here we focused on the widely-used thermal-

69   optical method, which separates carbonaceous components into two fractions with different thermal

70   stabilities and light absorption capacities, i.e., organic carbon (OC) and EC. The basis of the

71   separation includes two points: EC evolves form the filter at higher temperatures than OC, and the

72   removal of EC leads to a rapid increase in the filter transmittance and reflectance signals. A major

73   problem in this method is that a considerable fraction of OC could be transformed into char-OC,

74   which is difficult to be robustly distinguished from EC with respect to either thermal or optical

75   behavior. In addition, the amount and optical properties of char-OC were found to depend on the

76   temperature protocol deployed (Yu et al., 2002; Yang and Yu, 2002; Subramanian et al., 2006). This

77   to a large extent explained the EC discrepancies among various protocols. However, it remained

78   unclear how the charring process and thus the EC measurement were influenced by OC sources and

79   composition (Chiappini et al., 2014). In addition, to reduce or minimize the interference from char-

80   OC, several investigators have tried to remove a fraction of OC from the samples before thermal-

81   optical analysis, by extracting the filters using water, methanol or other solvents (Piazzalunga et al.,

82   2011; Giannoni et al., 2016; Lappi and Ristimäki, 2017; Aakko-Saksa et al., 2018; Hu et al., 2023).

83   However, inconsistent patterns were identified for the effects of OC removal on EC determination,

84   with evidences available for both an increase (e.g., Piazzalunga et al., 2011) and a decrease in EC

85   (e.g., Hu et al., 2023) after the extraction. The discussions above indicated that the thermal-optical

86   methods, including the practicability of sample pretreatment by extraction, merit further

87   investigations.

88   In this study, we compared carbonaceous aerosol results determined by different analytical as

89   well as sampling approaches, based on filter samples collected in Harbin, the northernmost megacity

90   in China. Compared to other megacities such as Beijing, Harbin is characterized by the frigid winter

91   (with an average temperature of about –20 °C in January) and the massive agricultural sector in

92   surrounding areas (i.e., the Songnen Plain in Northeast China). In addition, Harbin and other cities

93   in Northeast China have largely been overlooked in clean air actions and thus studies on haze, as

94   indicated by the limited observational data available (Liu et al., 2022). This lack of investigation

95   was partially responsible for the relatively slow decreasing rate (Xiao et al., 2022) and high exposure

96   risk (Wei et al., 2023) of $PM_{2.5}$ in this distinct region. Thus our study on measurement methods of

97   carbonaceous aerosols is expected to be a support for future efforts on the exploration of $PM_{2.5}$

98   sources in Northeast China, which are essential for further improving the regional air quality.

99   **2. Methods**

100   **2.1 Field sampling**

101         $PM_{2.5}$ samples were collected at an urban site in Harbin, i.e., on the campus of Harbin Institute

102   of Technology, during the winter and spring of 2021. The sampling was done by a mass flow

103   controlled high-volume sampler (TE-6070BLX-2.5-HVS; Tisch Environmental, Inc., OH, USA)

104   and a low-volume sampler (MiniVol; Airmetrics, OR, USA), operated using quartz-fiber filters (Pall

105   Corporation, NY, USA) at flow rates of 1.13 m^3/min and 5 L/min, respectively. The flow rates,

106   together with the particle-laden filter areas, could be translated into the face velocities of 46.34 and

107   7.35 cm/s for the high- and low-volume (HV and LV) samplers, respectively. This indicated that

108   when the two samplers were run in parallel, the HV-to-LV ratio of particle loading would be 6.3.

109   The 2021 winter campaign covered the entirety of January, the coldest month during that year

110   with an average temperature of −19 °C. In addition, the spring campaign was conducted during 10–

111   30 April of 2021, a period with frequent occurrences of agricultural fires (as indicated by the

112   satellite-based active fire detection results; Figure S1). For both seasons, the HV sampler was used

113   to collect daytime (09:00–16:00) and nighttime (21:00–05:00 of the next day) samples, while the

114   LV one was operated on a daily basis (~09:00–09:00 of the next day), leading to 24-h integrated

115   samples. Each LV sample generally corresponded to two HV samples, although the two samplers

116   were not exactly parallel. One reason for the relatively short sampling durations of HV was to avoid

117   high particle loadings that could prohibit proper filter transmittance measurement (Lappi and

118   Ristimäki, 2017).

119   **2.2 Laboratory analysis**

120   For both the HV and LV samples, two punches were prepared to determine OC and EC using

121   a thermal-optical carbon analyzer (DRI-2001; Atmoslytic Inc., CA, USA). One punch was directly

122   measured, while the other one was immersed in methanol (HPLC grade; Fisher Scientific Company

123   L.L.C., NJ, USA) for an hour without stirring or sonication, dried in air for another hour, and then

124   analyzed. All the pairs of untreated and extracted punches were measured using the IMPROVE-A

125   and NIOSH temperature protocols, both of which were operated with transmittance charring

126   correction (Figure 1). This correction approach was applied since the intensity of the filter

127   transmittance signal (I) has a clear association with EC, e.g., as assumed by the Aethalometer,

128   another widely used instrument for measuring black carbon. Inter-protocol comparisons showed

129   good repeatability for both the total carbon (TC) and optical attenuation (ATN) results (Figure 2),

130   demonstrating the robustness of the analyzer for detecting carbon and filter transmittance signals.

131   Here ATN was calculated as $\ln(I_{final}/I_{initial})$, where $I_{initial}$ and I_{final} indicate I measured at beginning

132   (i.e., when the particle-laden filter has not been heated) and end (i.e., when all the deposited carbon

133   has been combusted off the filter) of thermal-optical analysis, respectively. ATN was of interest

134   because it was closely related to EC loading (EC_s, in $\mu g/cm^2$), e.g., typically with a linear

135   dependence for relatively low EC_s levels (Chen et al., 2020; Liu et al., 2020). It should be noted that

for the parallel TC and ATN measurements by different protocols, the relative standard deviation

(RSD) levels indeed increased after the extraction, e.g., from ~2 to 5% and from ~2 to 4% for the

HV samples, respectively. However, the RSD levels, i.e., the uncertainties, were considered low

enough for both the untreated and extracted filters.

In addition, following the method developed by Hecobian et al. (2010), wavelength-resolved

light absorption coefficients (b_{abs}) of the methanol extracts, i.e., the dissolved brown carbon (BrC),

were measured using a spectrophotometer (Ocean Optics Inc., FL, USA) coupled with a 2.5-m long

liquid waveguide capillary cell (LWCC; World Precision Instruments, FL, USA). Inorganic ions and

levoglucosan were also determined for the HV and HV samples, by analyzing their water extracts

using a Dionex ion chromatography system (ICS-5000$^+$; Thermo Fisher Scientific Inc., MA, USA).
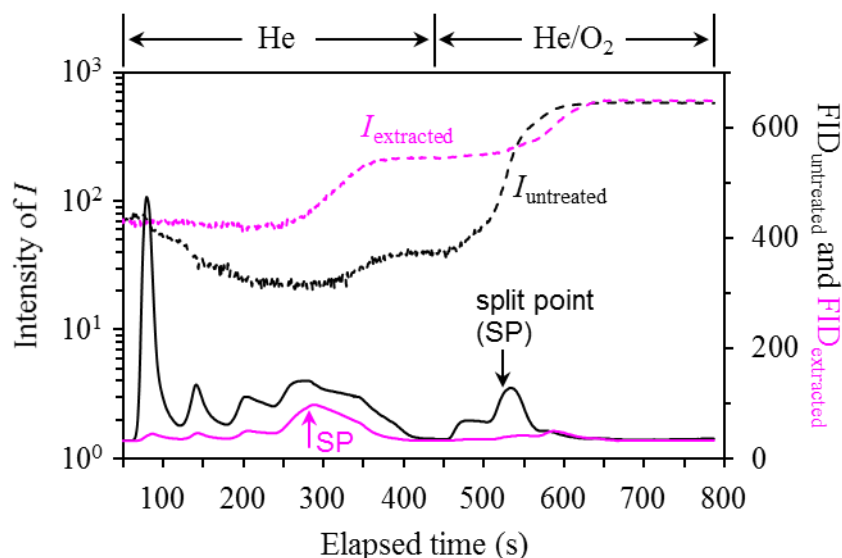
Figure 1. Thermograms measured using a pair of untreated and extracted HV filters. The sample
was collected during the daytime of 25 January, 2021. Temperature protocol used was NIOSH, in
which the filter was heated in a He (first to 870 ℃ stepwise and then cooled down to 550 ℃) and a
He/O$_2$ (from 550 to 890 ℃ stepwise) atmosphere sequentially. NIOSH had fixed durations for the
various heating stages and thus was preferred for the comparison of thermograms. I indicates the
filter transmittance signal; FID indicates the carbon signal, which was measured by a flame
ionization detector. The subscripts "untreated" and "extracted" distinguished the thermograms
measured before and after the extraction, while the split points of OC and EC were marked by the
arrows.
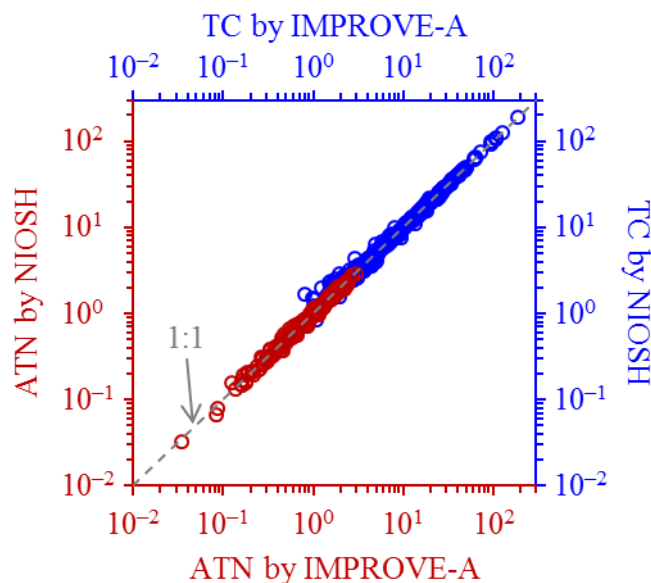
Figure 2. Comparisons of TC (in $\mu gC/cm^2$) and ATN (dimensionless) measured using different temperature protocols. Results from the HV and LV samples, both untreated and extracted, were combined for the comparisons. Linear regression of the NIOSH-based TC on that determined by IMPROVE-A led to a slope of 0.99 ± 0.00 ($r = 1.00$; intercept was set as zero). Similar regression results (i.e., slope = 0.99 ± 0.00; $r = 1.00$) were obtained for ATN. The good repeatabilities on one hand demonstrated the performance of carbon analyzer for measuring the carbon and laser transmittance signals, and on other hand indicated a homogeneous distribution of carbonaceous components for not only the untreated but also the extracted filters, i.e., a negligible disturbance of EC as well as other insoluble carbon by the extraction.

2.3 Open-access data

Meteorological data (e.g., temperature and relative humidity) and air quality data (e.g., $PM_{2.5}$, PM_{10} and CO) for the measurement periods were obtained with a time resolution of 1 h from Weather Underground (https://www.wunderground.com/) and the China National Environmental Monitoring Center (CNEMC; https://air.cnemc.cn:18007/), respectively.

3. Results and discussion

3.1 Evaluation of EC results from the winter campaign

A precondition for proper separation of OC and EC is that the filter transmittance signal (I) could properly reflect the formation of light-absorbing char-OC during the inert mode (which would result in a decrease in I), and the combustion, i.e., removal, of char-OC and EC during the oxidation

9

176   mode (which would result in an increase in I). An empirical approach to evaluate this precondition

177   is to examine the dependence of ATN on EC_s (Subramanian et al., 2006). A linear relationship was

178   typically observed for relatively low EC_s levels and in this case, the precondition was commonly

179   believed to be valid. However, the linearity did not necessarily extend when EC_s further increased,

180   since previous studies frequently found that the measured ATN could be considerably lower than

181   expected for heavily-loaded samples (Shen et al., 2013; Costa et al., 2016; Chen et al., 2020). The

182   deviation of ATN vs. EC_s dependence from linear relationship was usually termed the loading effect,

183   and a traditional explanation was that ATN became less sensitive to the variation of EC_s as filter

184   loading increased. An extreme case was observed during winter in Beijing, that the ATN values

185   were largely unchanged for heavily-loaded filters with TC varying between 150 and 300 $\mu gC/cm^2$

186   (Liu et al., 2019). For the samples showing non-linear ATN vs. EC_s dependence, their EC results

187   should be interpreted with caution.

188   We first investigated the relationship between ATN and EC_s for the wintertime HV samples,

189   focusing on the results from IMPROVE-A. For the untreated filters, ATN correlated linearly with

190   EC_s (leading to a regression slope of 42.8 $\pm$ 1.9 m^2/gC and a close-to-zero intercept; $r = 0.95$) when

191   the filters were lightly to moderately loaded, i.e., when the EC_s levels were below 5 $\mu gC/cm^2$ (Figure

192   3a). The physical meaning of the slope was the mass absorption efficiency (MAE) of black carbon,

193   but with artifacts such as that caused by the multiple scattering effect (Lack et al., 2014). The overall

194   impact of various artifacts results in an overestimation of MAE, typically by factors of ~3 (Knox et

195   al., 2009; Qin et al., 2018). The linearity determined for the EC_s range of below 5 $\mu gC/cm^2$ did not

196   hold for the more heavily loaded samples ($N = 3$, as highlighted by the solid circles in Figure 3a),

197   showing evidence for the loading effect. For the extracted samples, a linear correlation between

198 ATN and EC_s was also identified for relatively low EC loadings (Figure 3b), with a similar

199 relationship (i.e., a regression slope of 41.5 m²/gC and a close-to-zero intercept; $r = 0.95$) to that

200 derived from the untreated filters. However, it was noteworthy that EC_{max}, the upper limit of EC

201 loading for a linear ATN vs. EC_s dependence, was only 3 μgC/cm² for the extracted filters, much

202 lower than that determined for the untreated ones. Due to the shift of EC_{max}, 51% of the extracted

203 samples showed evidence for the loading effect, whereas this fraction was only 5% before extraction.

204
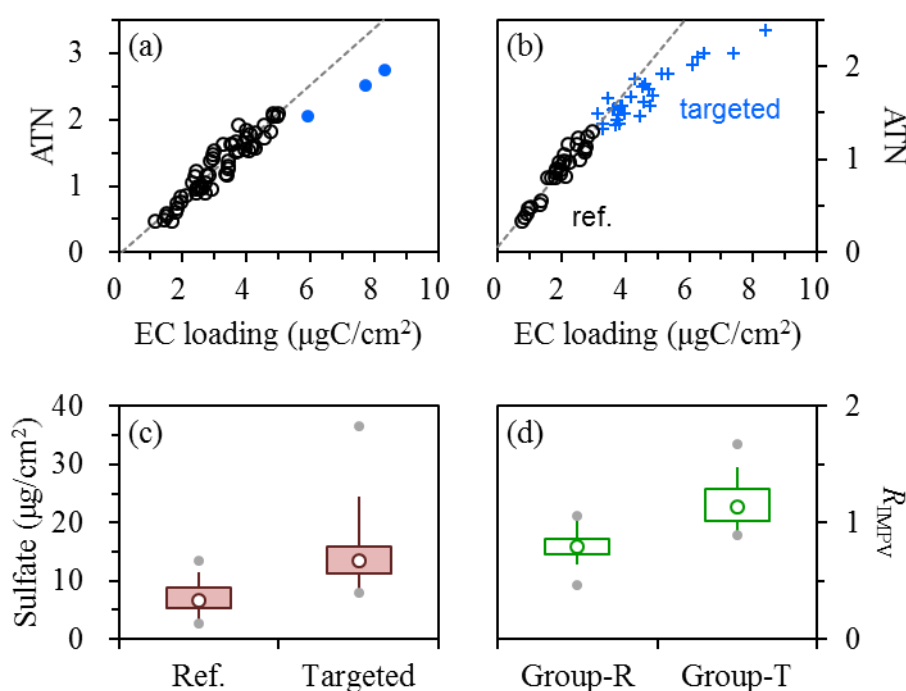
Figure 3. Relationships between ATN and EC loading, i.e., EC_s, for the **(a)** untreated and **(b)**
extracted HV filters collected in winter, using the IMPROVE-A protocol. Linear dependences were
observed for the untreated samples with EC_s below 5 μgC/cm² and for the extracted samples with
EC_s below 3 gC/cm², as indicated by the dashed lines in (a) and (b), respectively. Three untreated
samples had EC_s above 5 μgC/cm², as highlighted by the solid circles in (a). In (b), the extracted
filters showing non-linear ATN vs. EC_s dependence were termed the targeted samples;
correspondingly, the others were referred to as the reference ones (labelled as ref.). **(c)** Comparison
of sulfate loadings between the reference and targeted samples. **(d)** Comparison of the $EC_{extracted}$ to
$EC_{untreated}$ ratios, i.e., R_{IMPV}, between the reference and targeted groups of wintertime HV samples
(labelled as Group-R and Group-T, respectively). The targeted group indicated the targeted filters
and the corresponding untreated ones, while the reference group indicated the remaining pairs.
Lower and upper box bounds indicate the 25th and 75th percentiles, the whiskers below and above
the box indicate the 5th and 95th percentiles, the solid circles below and above the box indicate the
minimum and maximum, and the open circle within the box marks the median. All the EC results

219   involved were measured by IMPROVE-A.

220   The discussions above raised a question that why the extraction significantly reduced EC_{max}

221   for the HV samples. In principle, two factors could be responsible for the non-linear dependence of

222   ATN on EC_s, including gradual saturation of ATN with increasing filter loading (the traditional

223   explanation; Subramanian et al., 2006) and overestimation of EC mass. The EC_{max} of untreated

224   samples corresponded to an ATN of 2.1, indicating that the saturation was presumably not a concern

225   for the ATN results below this value. Regarding the extracted samples showing evidence for the

226   loading effect (i.e., the targeted samples), ATN stayed below 2.1 for nearly all of them (28 out of

227   31), thus their non-linear ATN vs. EC_s dependences should be primarily attributed to the

228   overestimation of EC mass rather than the saturation of ATN. Compared to the other extracted

229   samples, the targeted ones were characterized by substantially higher sulfate loadings (Figure 3c).

230   It was inferred that in addition to EC, the abundant sulfate was also a non-negligible contributor to

231   ATN (e.g., through backward scattering; Petzold et al., 2005; Collaud Coen et al., 2010). Thus when

232   the targeted samples were heated in the carbon analyzer, volatilization of sulfate would lead to a

233   decrease in ATN, i.e., an increase in filter transmittance signal. This was expected to result in a

234   premature split of OC and EC, and eventually an overestimation of EC. Other scattering components

235   such as nitrate and secondary organic aerosol (SOA) were not discussed here, since they were

236   typically considered soluble in methanol and should be absent in the extracted filters.

237   Comparison of EC between the targeted samples and the corresponding untreated ones (i.e.,

238   the targeted group) showed an overall increasing trend after the extraction (Figure 3d). For these

239   pairs of wintertime HV filters, the ratio of $EC_{extracted}$ (i.e., EC measured in the extracted samples) to

240    $EC_{untreated}$ (i.e., EC measured in the untreated samples) averaged 1.16 ±0.20. The extraction-induced

241   increase in EC coincided with the overestimation of elemental carbon mass by $EC_{extracted}$, which was

242   inferred to be associated with the presence of abundant sulfate in the extracted filters.

243   For the other pairs of wintertime HV samples (i.e., the reference group), the $EC_{extracted}$ to

244      $EC_{untreated}$ ratios averaged 0.80 ± 0.12, pointing to a decrease in EC after the extraction (Figure 3d).

245   This was also the case for all the LV samples collected during the winter campaign, with comparable

246      $EC_{extracted}$ to $EC_{untreated}$ ratios (averaging 0.78 ± 0.12). Here the LV samples were not divided into

247   subgroups because non-linear dependence of ATN on EC_s was identified neither before nor after the

248   extraction (Figure S2). Given that the loss of insoluble carbon (e.g., EC) was negligible for our

249   extraction procedures (Figure 2 and Cheng et al., 2024), the extraction-induced decrease of EC

250   likely pointed to the underestimation of elemental carbon mass by $EC_{extracted}$. A common feature for

251   the HV samples in the reference group and the entirety of the LV samples was the relatively low

252   sulfate loadings. Cheng et al. (2024) inferred that small amounts of sulfate likely favored the

253   transmission of light through the extracted filters (e.g., by forward scattering; Petzold et al., 2005;

254   Collaud Coen et al., 2010). In this case, when the extracted samples were heated during thermal-

255   optical analysis, volatilization of sulfate would induce a drop of filter transmittance signal, which

256   could not be distinguished from that caused by the formation of char-OC. This was expected to

257   result in an overcorrection for char-OC, i.e., an underestimation of EC.

258   The contrasting $EC_{extracted}$ to $EC_{untreated}$ ratios observed for the two groups of wintertime HV

259   samples suggested that the influence of sulfate on the transmittance signal of the extracted filter was

260   likely loading-dependent. The influence was inferred to be dominated by backward scattering with

261   relatively high sulfate loadings (e.g., for the targeted group), whereas by forward scattering when

262   sulfate was less abundant (e.g., for the reference group). This inference was supported by the

263   comparison of evolution patterns of filter transmittance signal under different sulfate loadings

264   (Figure 4). For the extracted filter with abundant sulfate (i.e., Sample-A in Figure 4), the

265   transmittance signal was largely unchanged during the He mode despite the sufficient organic

266   carbon loading. Correspondingly, the operationally-defined char-OC only accounted for a relatively

267   small fraction of the carbon evolving during the He/O$_2$ mode (i.e., He/O$_2$ carbon). A possible

268   explanation was that as the sample was heated, the drop of I induced by char-OC was compensated

269   by the increase of I due to the reduction in sulfate-driven backward scattering. For the extracted

270   filter with relatively small amount of sulfate (i.e., Sample-B in Figure 4), however, the transmittance

271   signal decreased significantly during the He mode, and the char-OC contribution to He/O$_2$ carbon

272   became more considerable correspondingly. Given the much lower organic carbon loading for this

273   sample (e.g., ~70% lower than Sample-A), the decrease of I was likely contributed by not only the

274   formation of char-OC but also the reduction in sulfate-driven forward scattering. The EC$_{extracted}$

275   results appeared to be biased by different artifacts in the high- and low-sulfate cases, resulting in

276   overestimations or underestimations of elemental carbon mass, respectively. The sulfate-induced

277   artifacts for EC$_{extracted}$ could be more directly reflected by the positive dependence of the EC$_{extracted}$

278   to EC$_{untreated}$ ratio on sulfate loading. As shown in Figure 5, the turning point for the artifact shifting

279   from an underestimation to overestimation of elemental carbon mass by EC$_{extracted}$ occurred in the

280   sulfate loading range of 10–15 μg/cm^2. Figure 5 also suggested that the artifacts for EC$_{extracted}$ were

281   difficult to be accounted for, e.g., by a constant correction factor. This prohibited the use of EC$_{extracted}$

282   for further analysis of aerosol composition and sources.
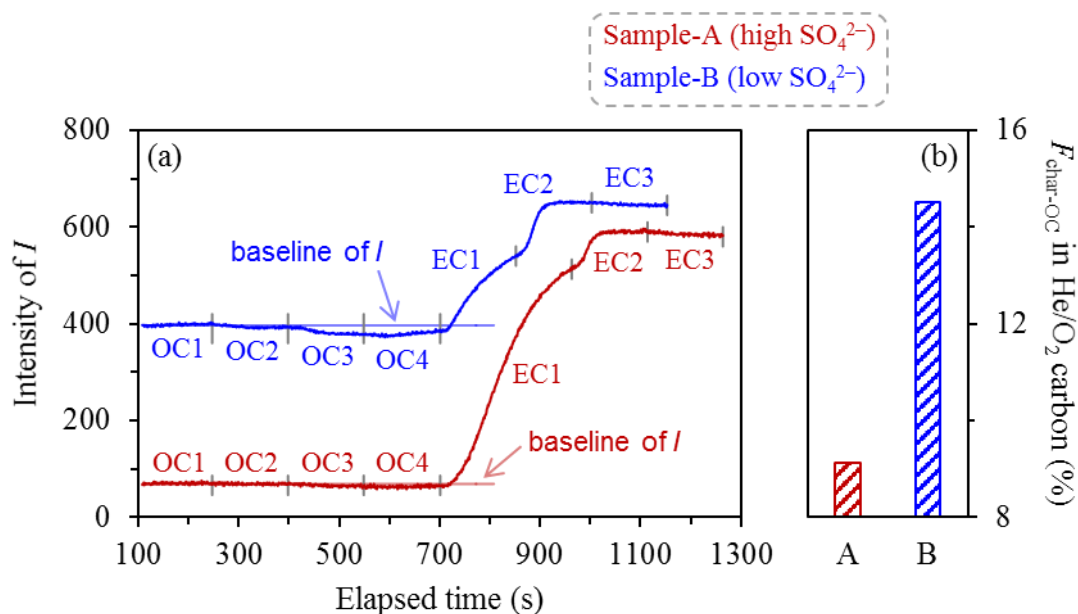
Figure 4. Comparisons of **(a)** the evolution patterns of filter transmittance signal (I) and **(b)** the fractions of char-OC (i.e., $F_{\text{char-OC}}$) in He/O$_2$ carbon for two extracted HV samples with relatively high and low sulfate loadings (namely Sample-A and Sample-B, respectively). The two samples were collected during the daytime of 25 January and the nighttime of 6 January, 2021, respectively. They had sulfate loadings of 13.21 and 3.29 μg/cm^2, and organic carbon loadings of 3.10 and 0.86 μgC/cm^2, respectively. The temperature protocol used was IMPROVE-A, in which the filter was first heated to 580 ℃ in a He atmosphere and then to 840 ℃ in a He/O$_2$ atmosphere. The two modes had 4 (i.e., OC1 to OC4) and 3 (i.e., EC1 to EC3) heating stages, respectively. He/O$_2$ carbon indicated the amount of carbon evolving during the oxidizing mode, and was typically comprised of char-OC and EC for IMPROVE-A.
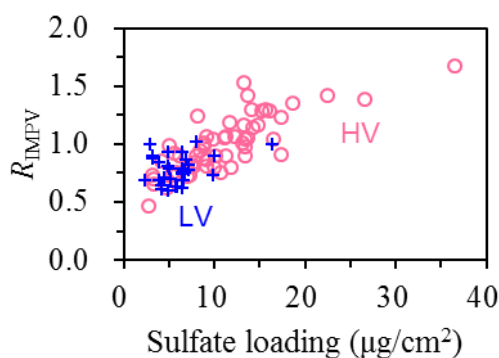

Figure 5. Dependence of R_{IMPV}, i.e., the EC$_{\text{extracted}}$ to EC$_{\text{untreated}}$ ratio determined by IMPROVE-A, on sulfate loading in winter. Consistent trends were observed by the HV and LV samples. The relatively wide range of R_{IMPV} (approximately 0.5–1.5) provided solid evidence for the invalidation of the EC$_{\text{extracted}}$ to EC$_{\text{untreated}}$ ratio as an indicator for the extraction-induced loss of EC.

For the untreated filters, ATN exhibited a strong linear correlation with EC$_\text{s}$ for both HV and

LV, with three heavily-loaded HV samples as the only exception. Actually, for the three samples,

15

301 　　their ATN vs. EC_s relationships did not deviate markedly from the regression line determined for

302 　　the lower EC_s loadings. Therefore, we suggested that when applying IMPROVE-A to the winter

303 　　samples, the measurement uncertainties should be less significant for $EC_{untreated}$ compared to

304 　　$EC_{extracted}$.

305 　　　　The same conclusion could be reached by interpreting the OC to EC ratios (OC/EC). It has

306 　　been widely accepted that OC/EC depended strongly on SOA formation, after excluding the events

307 　　impacted by irregular emissions such as fireworks and open burning. Such events were not evident

308 　　throughout the winter campaign, and thus OC/EC was expected to increase with the enhancement

309 　　of secondary aerosol production. Here we used the relative abundance of secondary inorganic ions

310 　　(sulfate, nitrate and ammonium, i.e., SNA) compared to carbon monoxide (a typical primary

311 　　species), i.e., the SNA/CO ratio, as an indicator for the significance of secondary aerosols. A benefit

312 　　of using SNA/CO was that it was independent of EC measurement. The OC/EC ratio corresponding

313 　　to $EC_{untreated}$ [i.e., $(OC/EC)^*$] was determined directly by the thermal-optical results from the

314 　　untreated samples. For $EC_{extracted}$, the corresponding OC/EC [i.e., $(OC/EC)^\#$] was calculated as

315 　　$(TC_{untreated} - EC_{extracted})/ EC_{extracted}$, where $TC_{untreated}$ indicates the total carbon concentration

316 　　measured before the extraction. As shown in Figure 6 for the wintertime HV samples, $(OC/EC)^*$

317 　　exhibited reasonable accordance with SNA/CO ($r = 0.72$) but $(OC/EC)^\#$ did not ($r = 0.02$). The clear

318 　　association between $(OC/EC)^*$ and SNA/CO, which was also supported by the results from LV ($r =$

319 　　0.66; Figure S3), provided additional evidence for the robustness of $EC_{untreated}$ determined by
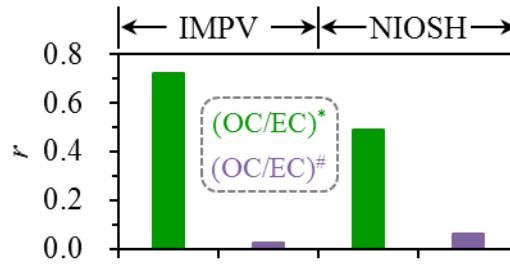
320 　　IMPROVE-A.

Figure 6. Comparison of *r* values derived from the linear regressions of various OC/EC estimations on SNA/CO, based on the wintertime HV samples. IMPV indicates the IMPROVE-A temperature protocol. A total of four sets of OC/EC ratios were determined using different protocols and pre-treatment approaches. The OC/EC ratio measured by the untreated samples using IMPROVE-A, i.e., the IMPV-based (OC/EC)*, exhibited the strongest association with SNA/CO.

Compared to IMPROVE-A, NIOSH led to weaker correlations between (OC/EC)* and SNA/CO, as indicated by the smaller *r* values determined (0.49 vs. 0.72 for HV and 0.18 vs. 0.66 for LV; Figures 4 and S3). In addition, the NIOSH-based (OC/EC)# did not exhibit apparent dependence on SNA/CO either ($r = 0.06$ and 0.34 for HV and LV, respectively). Thus Figures 6 and S3 clearly reflected the limitations of NIOSH-based OC/EC and thus NIOSH-based EC, further highlighting the benefit of using EC$_{untreated}$ determined by IMPROVE-A.

3.2 Evaluation of EC results from the spring campaign

In this section we evaluated the EC results from April, also starting with the HV samples analyzed by IMPROVE-A. To highlight the role of agricultural fires, we first separated the April samples into two groups (namely the fire-impacted and typical samples), which were characterized by considerable and insignificant impacts of open burning, respectively. As described in Supporting Information, the criteria for fire-impacted samples could be simplified as a levoglucosan to TC$_{untreated}$ ratio (f_{LG}; on a basis of carbon mass) of above 1.8%, based on a synthesis of f_{LG}, the levoglucosan to water-soluble potassium ratio (LG/K$^+$) and satellite-based fire hotspots (Figure S4). Before filter extraction, the dependence of ATN on EC$_s$ could be approximated by a liner function (with a slope of 33.4 ± 1.5 m^2/gC and a close-to-zero intercept; $r = 0.97$) for all the typical samples

343   and the majority of the fire-impacted ones (Figure 7a), leading to an EC_{max} of 8 μgC/cm^2. For three

344   of the fire-impacted samples, EC_s exceeded this threshold value and the ATN vs. EC_s relationships

345   were found to deviate significantly from the regression line, especially for the two samples with EC_s

346   above 10 μgC/cm^2 (as highlighted in Figure 7a).

347
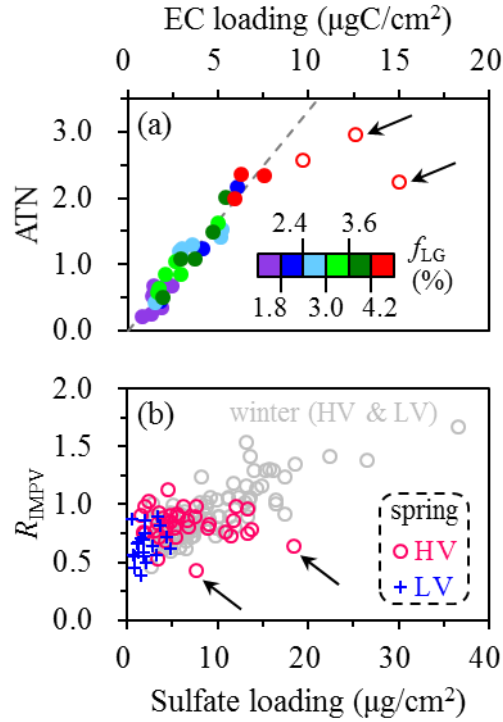
Figure 7. (a) Dependence of ATN on EC loading (EC_s) for the untreated HV samples collected in spring, color-coded by f_{LG} levels. Samples with linear and non-linear ATN vs. EC_s dependence are shown by the solid and open circles, respectively. f_{LG} values higher than 1.8% indicated significant impacts of agricultural fires. **(b)** Dependence of R_{IMPV}, i.e., the $EC_{extracted}$ to $EC_{untreated}$ ratio, on sulfate loading in spring. Results from winter were also shown for comparison. In general, a consistent relationship was observed between R_{IMPV} and sulfate loading for the samples, including both HV and LV, from different seasons. Two HV samples collected in spring were identified as outliers, as highlighted by the arrows. The outlier samplers were also highlighted in (a), corresponding to the two points showing significant non-linear dependences of ATN on EC loading. All the EC results involved were measured by IMPROVE-A.

358   To elucidate factors responsible for the observed non-linear dependence of ATN on EC_s, we

359   compared EC results from the untreated and extracted filters. Given the relatively low sulfate

360   loadings observed throughout April (Figure 7b), it was with expectation that EC generally decreased

361   after the extraction. After excluding the results from two outliers (Figure 7b), the $EC_{extracted}$ to

362     $EC_{untreated}$ ratios averaged 0.84 ±0.11, comparable to results from the reference group in winter. The

363   two outlier samples, which were collected on the nights of April 10 and 20, 2021, showed $EC_{extracted}$

364   to $EC_{untreated}$ ratios of as low as 0.64 and 0.43, respectively. Such significant extraction-induced

365   decreases in EC could hardly be explained by the interference from sulfate in thermal-optical

366   analysis of the extracted filters (Figure 7b). Instead, the two outlier samples were found to show

367   several noteworthy features: (i) they corresponded to the two samples showing significant non-

368   linear ATN vs. EC_s dependences before the extraction (Figure 7a); (ii) their f_{LG} levels were at the

369   higher end of the fire-impacted samples (with levoglucosan concentrations exceeding 7 μg/m^3),

370   indicating extremely strong impacts of open burning (Figure 7a); (iii) their LG/K^+ ratios (> 1.7)

371   were also at the higher end of the fire-impacted samples, which were characteristic of the emissions

372   from smoldering combustion (Gao et al., 2003; Sullivan et al., 2019); (iv) their ATN decreased

373   apparently after the extraction, by ~1.0 which were about one order of magnitude higher than results

374   from the typical samples (~0.1). Thus it was inferred that $EC_{untreated}$ of the outlier samples likely

375   involved some light-absorbing organic compounds (i.e., BrC) emitted by agricultural fires with

376   relatively low combustion efficiencies, and the absorption capacities of these organics were strong

377   enough to make them a considerable contributor to ATN measured at 632 nm. Indeed, the BrC-

378   related overestimation of elemental carbon mass was expected to be reduced considerably after the

379   extraction. However, such overestimation seemed significant only for the two outlier samples

380   (Figure 7a). In addition, recalling the lower-than-one $EC_{extracted}$ to $EC_{untreated}$ ratios observed for the

381   other April samples (i.e., the sulfate-related artifact raised for the extracted filters), the methanol

382   extraction actually brought little benefit for the determination of EC by IMPROVE-A.

383 Unlike HV, all the LV samples showed a consistent relationship between ATN and EC_s before

384 the extraction (Figure S5). It appeared that the strongly absorbing organics that could interfere EC

385 measurement were mainly concentrated in some agriculture-fire smoke emitted at night (as

386 indicated by the two outlier HV samples), whereas their influence on EC determination was

387 considerably weakened for the 24-h integrated LV samples. Thus the linear ATN vs. EC_s dependence,

388 which was valid for all the untreated LV samples analyzed by IMPROVE-A, provided little evidence

389 for the necessity of methanol extraction.

390 We also investigated the OC/EC vs. f_{LG} relationship for the HV samples collected in April.

391 Open burning was considered to be favorable for the increase of ambient OC/EC, since the aerosols

392 emitted were frequently found to be almost entirely organic (Liu et al., 2016; Garofalo et al., 2019;

393 Gkatzelis et al., 2024). Then it was not surprising to observe a moderate correlation between

394 $(OC/EC)^*$ and f_{LG} ($r = 0.59$; Figure 8), i.e., an increasing trend of $(OC/EC)^*$ with stronger impacts

395 of agricultural fires. In addition, $(OC/EC)^*$ also depended moderately on SNA/CO ($r = 0.49$; Figure

396 8). This was with expectation as well, given the observational evidence on the concurrent

397 enhancements of secondary inorganic and organic aerosols (e.g., Liu et al., 2020; Cheng et al., 2022).

398 Replacing $(OC/EC)^*$ with $(OC/EC)^{\#}$ did not effectively strengthen the association of OC/EC with

399 f_{LG} or SNA/CO (Figure 8). This conclusion also held for the LV samples (Figure 8). In summary,

400 we did not observe additional evidence supporting the incorporation of methanol extraction with
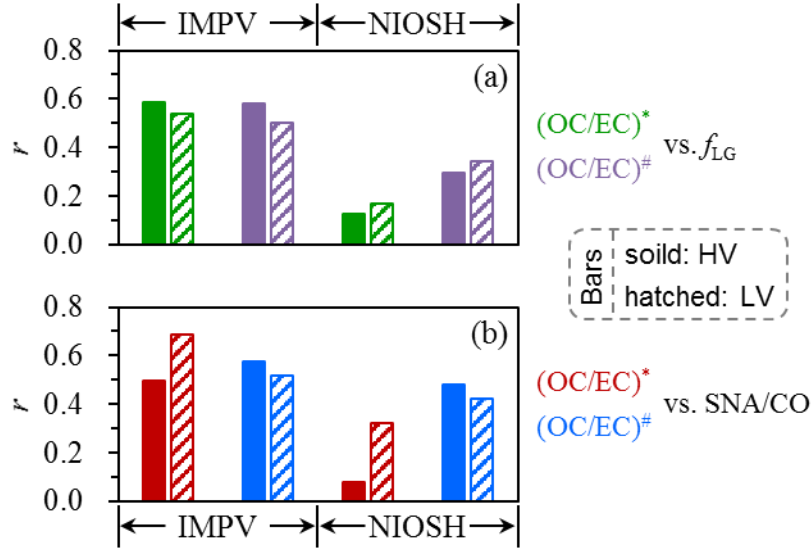
401 IMPROVE-A.

Figure 8. Comparisons of r values derived from the linear regressions of various OC/EC estimations on **(a)** f_{LG} and **(b)** SNA/CO, based on the spring samples. IMPV indicates the IMPROVE-A temperature protocol. Results from the HV and LV filters are shown by solid and hatched bars, respectively. For both HV and LV, a total of four sets of OC/EC ratios were determined using different protocols and pre-treatment approaches. In general, OC/EC ratios measured by the untreated samples using IMPROVE-A, i.e., the IMPV-based (OC/EC)*, exhibited reasonable associations with aerosol sources. Using other OC/EC estimations failed to or did not effectively enhance the associations.

Compared to (OC/EC)* determined by IMPROVE-A, the NIOSH-based (OC/EC)* and (OC/EC)# were less indicative of aerosol sources which could be reflected by f_{LG} and SNA/CO. This was the case for both the HV and LV samples (Figure 8). Based on the discussions above, EC$_{untreated}$ determined by IMPROVE-A (EC*) was also recommended for the conditions with prevalence of agricultural fires (i.e., April), in line with the conclusion derived for winter. In addition, it should be kept in mind that EC* could overestimate elemental carbon mass due to the interference from strongly absorbing BrC. However, such overestimation was generally uncommon, i.e., was significant only for some nighttime samples under extremely strong influences of low-efficiency agricultural fires (as indicated by the two HV samples identified as outliers; Figure 7).

3.3 Comparison of measurement results from the HV and LV samplers

As mentioned in the Methods section, each LV sample corresponded to a pair of daytime and

nighttime HV samples, indicating that measurement results from the HV samples could be averaged

and then compared to those determined by LV. Here the inter-sampler comparison was performed

for several components that are of broad interest in field observations, including elemental and

organic carbon, secondary inorganic ions (sulfate, nitrate and ammonium), other water-soluble ions

(potassium and chloride), organic tracer for biomass burning (levoglucosan), BrC mass

concentration and light absorption coefficient. Based on the evaluation results in previous sections,

EC^* and the corresponding OC, i.e., OC^* (measured before the extraction using IMPROVE-A), were

selected for the comparison. In addition, following Cheng et al. (2024), BrC mass was calculated as

the difference in TC between the untreated and extracted filters, while BrC absorption was

investigated at a wavelength of 365 nm, i.e., $(b_{abs})_{365}$.

As shown in Figure 9, the two samplers generally led to comparable measurement results for

all the species investigated. For example, the LV-to-HV ratios typically fell within the range of 0.8–

1.2, i.e., results from the two samples generally agreed within $\pm 20\%$. However, it was noticed that

K^+ was the only component with the majority of the LV results lower than HV. In addition, the LV-

to-HV ratio of K^+ was found to depend positively on the ratio of $PM_{2.5}$ to PM_{10} (Figure 10a). The

$PM_{2.5}$ to PM_{10} ratio was strongly associated with the influence of dust, typically exhibiting a

decreasing trend as the impact of dust became stronger (Putaud et al., 2010). Thus the events with

decreased LV-to-HV ratios of K^+ (all of which occurred in spring) presumably coincided with dust

episodes, when relatively large particles were expected to be a non-negligible contributor to K^+

(Wang et al., 2014a). Then a likely cause for the dependence shown in Figure 8a was that the

impactor performances (e.g., the size-cut curves) were not exactly the same for the two samplers,

such that some relatively large particles, if present, could be more effectively collected onto the HV

444   filters compared to LV.
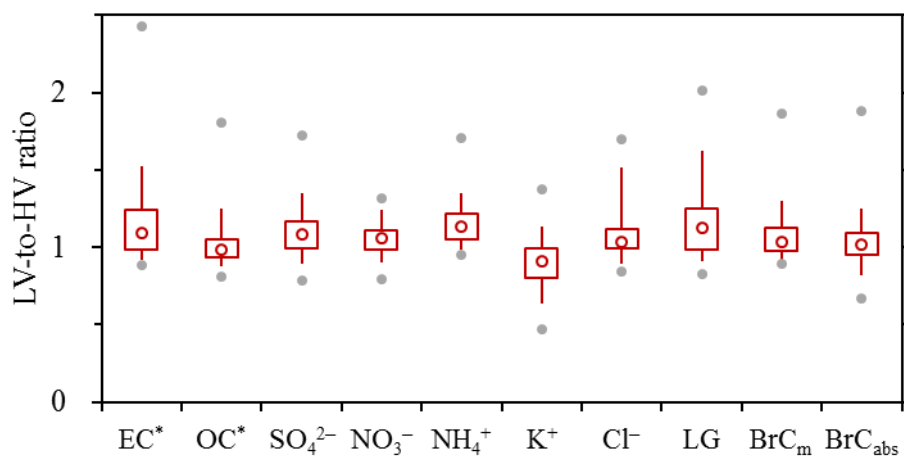
Figure 9. The LV-to-HV ratios determined for various species. BrC_m and BrC_{abs} indicate the mass concentration and $(b_{abs})_{365}$ of brown carbon, respectively.
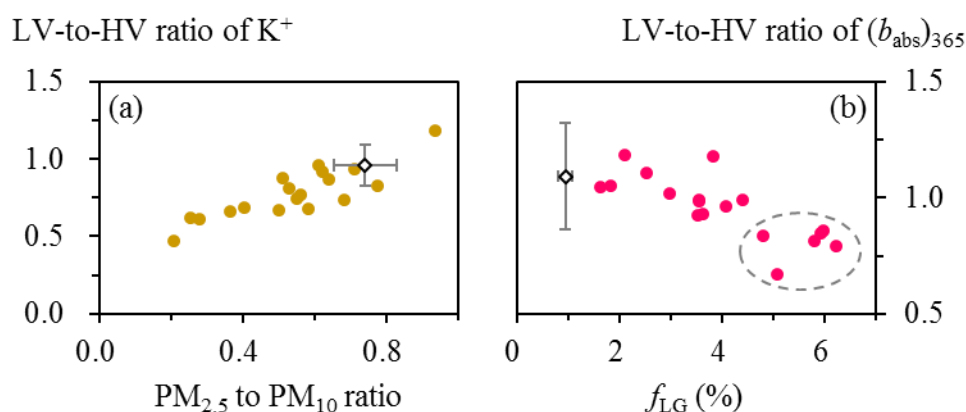
Figure 10. **(a)** Dependence of the LV-to-HV ratio of K^+ on the $PM_{2.5}$ to PM_{10} ratio. **(b)** Dependence of the LV-to-HV ratio of $(b_{abs})_{365}$ on f_{LG}. Results from spring are shown on a sample-by-sample basis, as indicated by the solid circles. For winter, only the average results are shown as indicated by the diamonds. In (b), the events with substantially lower LV-to-HV ratios of $(b_{abs})_{365}$ are highlighted by the dashed oval.

454   In addition, it was noticed that although the two samplers led to generally comparable $(b_{abs})_{365}$

455   results, the corresponding LV-to-HV ratios decreased substantially (e.g., down to 0.67) for the

456   episodes with extremely strong impacts of agricultural fires (Figure 10b). A possible explanation

457   was that some fire-emitted chromophores were associated with relatively large particles that would

458   be more effectively collected onto the HV filters. Although these chromophores represented an

459   important contributor to BrC absorption, their influence on BrC mass was likely insignificant, as

460   indicated by the little influence of agricultural fires on the LV-to-HV ratio of BrC mass (Figure S6).

461   Finally, it should be noted that for the species except K^+ and $(b_{abs})_{365}$, their LV-to-HV ratios

462   still showed different patterns of distribution (Figure 9). Analytical uncertainties should be partially

463   responsible, e.g., as indicated by the more significant variations in the LV-to-HV ratios of EC^*

464   compared to those of OC^*. Another likely cause was that the sampling duration of a given LV sample

465   (24 hours) actually did not equal that of the corresponding HV (15 hours), which would result in

466   different LV-to-HV ratios for the species with different diurnal cycles. In summary, many factors

467   could be responsible for the inter-sampler discrepancies shown in Figure 9. Typically, the overall

468   effects of these factors were higher LV-based concentrations than HV, with median LV-to-HV ratios

469   concentrating in a relatively narrow range of 1−1.15. However, this comparability may not always

470   hold. A possible explanation was that the impactor performances were more or less different

471   between the two samplers, thus for specific components such as K^+ and some fire-emitted

472   chromophores, this difference could exert a significant influence on their sampling.

473   **4. Conclusions and implications**

474   For the first time, EC results were compared among different sampling and analytical

475   approaches based on field observations in Northeast China. Two samplers with flow rates of 1.13

476   m^3/min and 5 L/min were operated together during two distinct seasons, whereas thermal-optical

477   analysis was performed by applying different protocols to both the untreated and extracted filters.

478   Results from different seasons jointly suggested that $EC_{extracted}$ measured by IMPROVE-A (i.e.,

479   IMPV) was biased by complex artifacts associated with sulfate. The IMPV-based $EC_{extracted}$ tended

480   to underestimate elemental carbon mass when sulfate was less abundant, whereas overestimations

481   were evident at sufficiently high loadings of sulfate. The turning point for the artifact shifting from

482   an underestimation to overestimation occurred in the sulfate loading range of 10–15 $\mu g/cm^2$. Such

483   high sulfate loadings were rarely encountered by the LV samples and thus the corresponding IMPV-

484   based EC typically decreased after the extraction (by ~20%). For the HV samples, their sulfate

485   covered a wide range of ~2–35 $\mu g/cm^2$ during winter and in this case, the extraction-induced

486   changes in EC usually varied between −50% and +50% for the IMPV-based results. In addition to

487   the complex sulfate-related artifacts, another problem identified for the IMPV-based $EC_{extracted}$ was

488   that the corresponding OC/EC ratio sometimes exhibited no association with the SNA/CO ratio,

489   which was used as an indicator for the significance of secondary aerosol production. The NIOSH-

490   based OC/EC ratios, determined by either $EC_{extracted}$ or $EC_{untreated}$, had the same problem. Then the

491   IMPV-based $EC_{untreated}$ (EC^*) was recommended, as the corresponding OC/EC could always be

492   reasonably linked to aerosol sources, e.g., secondary aerosol formation in winter and agricultural

493   fire impacts (as reflected by f_{LG}) in spring.

494   Inter-sampler comparisons were performed for various species that are of broad interest in field

495   observations, including EC^*. Although the flow rates differed by more than two orders of magnitude

496   between the two samplers, the LV and HV generally led to comparable measurement results for the

497   majority of the species, with the median LV-to-HV ratios falling within a relatively narrow range of

498   1–1.15.

499   This study also raised two points that merit attentions. The first is that the IMPV-based

500    $EC_{untreated}$, which was suggested for investigations on aerosol sources, might overestimate elemental

501   carbon mass under extremely strong impacts of open burning. This problem was attributed to

502   strongly absorbing BrC emitted by agricultural fires with relatively low combustion efficiencies.

503   Although uncommon for the ambient samples in Harbin (a megacity located in a main agricultural

504   region in China), this problem could introduce substantial uncertainties to the emission factors and

505   thus inventories of biomass burning. We suggested that a key step to refine the EC measurement

506   results was to concurrently minimize the inferences from strongly absorbing BrC and scattering

507   components. Methanol extraction followed by water extraction of filter samples was expected to be

508   a practical approach, which was worthy of further evaluations.

509   The second point was that some specific components should be interpreted with caution, even

510   when comparing their measurement results from samplers with the same nominal cut-point. Our

511   observational results indicated that some relatively large particles, if present, could be more

512   effectively collected by the high-volume $PM_{2.5}$ sampler compared to the low-volume one. This

513   problem was attributed to the fact that the inlet performances (e.g., the size-cut curve) could not be

514   exactly the same between the HV and LV $PM_{2.5}$ samplers. Among the various species involved in

515   this study, this problem affected the measurements of K^+ as well as some fire-emitted chromophores

516   in the fine mode. Thus we suggested that the K^+ results derived from different $PM_{2.5}$ samplers may

517   not be directly comparable. In addition, although we could not quantitatively determine the dust

518   contribution to K^+ measured by the high-volume $PM_{2.5}$ sampler, K^+ should be used with caution as

519   a biomass burning tracer for source apportionment studies relying on the HV-based observations.

520   By evaluating the observational results from different measurement approaches for species

521   commonly used in source apportionment, this study contributed to the understanding of aerosol

522   sources in Northeast China and thus the development of efficient haze pollution control strategies.

523   Using the recommended OC and EC results together with levoglucosan (rather than K^+) as the

524   biomass burning tracer, positive matrix factorization (PMF) analysis was performed for the 2020–

2021 heating season based on a total of ~200 LV samples (including those involved in this study; Cheng et al., 2024). The concentrations of primary OC resolved were found to be in reasonable agreement with those predicted by an air quality model, when agricultural fires were absent. The consistency laid the foundation for the control policy focusing on primary aerosols. Cheng et al. (2024) also found that the model failed to reproduce the observed SOA levels, with large underestimations (by ~80%). Thus the observation-based source apportionment results were currently irreplaceable for evaluating the benefits of reducing SOA precursors. In summary, this study highlighted the importance of inter-method comparison for aerosol components (e.g., EC and K^+) that are of broad interest in field observations. Such efforts are expected to be more urgently needed for Northeast China, since this distinct region was recently targeted by the latest national-level pollution control policy in China (State Council, 2021) and thus is facing stronger demand for reducing $PM_{2.5}$.

Data availability. Data are available from the corresponding author upon request (jiumengliu@hit.edu.cn).

Author contributions. YC and JL designed the study and prepared the paper, with inputs from all the co-authors. YZ, ZZ and XC carried out the experiments.

Competing interests. The authors declare that they have no conflict of interest.

Disclaimer. Publisher's note: Copernicus Publications remains neutral with regard to jurisdictional claims made in the text, published maps, institutional affiliations, or any other geographical representation in this paper. While Copernicus Publications makes every effort to include appropriate place names, the final responsibility lies with the authors.

553   **References**

554   Aakko-Saksa, P., Koponen, P., Aurela, M., Vesala, H., Piimäkorpi, P., Murtonen, T., Sippula, O.,

555   Koponen, H., Karjalainen, P., Kuittinen, N., Panteliadis, P., Rönkkö, T., and Timonen, H.:

556   Considerations in analysing elemental carbon from marine engine exhaust using residual,

557   distillate and biofuels, *J. Aerosol Sci.*, 126, 191–204, 2018.

558   Andela, N., Morton, D. C., Schroeder, W., Chen, Y., Brando, P. M., and Randerson, J. T.: Tracking

559   and classifying Amazon fire events in near real time, *Sci. Adv.*, 8, eabd2713, 2022.

560   Andreae, M. O., and Gelencsér, A.: Black carbon or brown carbon? The nature of light-absorbing

561   carbonaceous aerosols, *Atmos. Chem. Phys.*, 6, 3131–3148, 2006.

562   Buffaloe, G. M., Lack, D. A., Williams, E. J., Coffman, D., Hayden, K. L., Lerner, B. M., Li, S. M.,

563   Nuaaman, I., Massoli, P., Onasch, T. B., Quinn, P. K., and Cappa, C. D.: Black carbon

564   emissions from in-use ships: a California regional assessment, *Atmos. Chem. Phys.*, 14, 1881–

565   1896, 2014.

566   Cavalli, F., Viana, M., Yttri, K. E., Genberg, J., and Putaud, J. P.: Toward a standardized thermal-

567   optical protocol for measuring atmospheric organic and elemental carbon: the EUSAAR

568   protocol, *Atmos. Meas. Tech.*, 3, 79–89, 2010.

569   Chakrabarty, R. K., Shetty, N. J., Thind, A. S., Beeler, P., Sumlin, B. J., Zhang, C. C., Liu, P., Idrobo,

570   J. C., Adachi, K., Wagner, N. L., Schwarz, J. P., Ahern, A., Sedlacek, A. J., Lambe, A., Daube,

571   C., Lyu, M., Liu, C., Herndon, S., Onasch, T. B., and Mishra, R.: Shortwave absorption by

572   wildfire smoke dominated by dark brown carbon, *Nat. Geosci.*, 16, 683–688, 2023.

573 Chang, X., Zhao, B., Zheng, H. T., Wang, S. X., Cai, S. Y., Guo, F. Q., Gui, P., Huang, G. H., Wu,
574   D., Han, L. C., Xing, J., Man, H. Y., Hu, R. L., Liang, C. R., Xu, Q. C., Qiu, X. H., Ding, D.,
575   Liu, K. Y., Han, R., Robinson, A. L., and Donahue, N. M.: Full-volatility emission framework
576   corrects missing and underestimated secondary organic aerosol sources, *One Earth*, 5, 403–
577   412, 2022.

578 Chen, P. F., Kang, S. C., Tripathee, L., Ram, K., Rupakheti, M., Panday, A. K., Zhang, Q., Guo, J.
579   M., Wang, X. X., Pu, T., and Li, C. L.: Light absorption properties of elemental carbon (EC)
580   and water-soluble brown carbon (WS-BrC) in the Kathmandu Valley, Nepal: a 5-year study,
581   *Environ. Pollut.*, 261, 114239, 2020.

582 Cheng, J., Tong, D., Zhang, Q., Liu, Y., Lei, Y., Yan, G., Yan, L., Yu, S., Cui, R. Y., Clarke, L., Geng,
583   G. N., Zheng, B., Zhang, X. Y., Davis, S. J., and He, K. B.: Pathways of China's $PM_{2.5}$ air
584   quality 2015-2060 in the context of carbon neutrality, *Natl. Sci. Rev.*, 8, nwab078, 2021.

585 Cheng, Y., Cao, X. B., Yu, Q. Q., Liu, J. M., Ma, W. L., Qi, H., Zhang, Q., and He, K. B.: Synergy
586   of multiple drivers leading to severe winter haze pollution in a megacity in Northeast China,
587   *Atmos. Res.*, 270, 106075, 2022.

588 Cheng, Y., Cao, X. B., Zhu, S. Q., Zhang, Z. Q., Liu, J. M., Zhang, H. L., Zhang, Q., and He, K. B.:
589   Exploring the sources of light-absorbing carbonaceous aerosols by integrating observational
590   and modeling results: insights from Northeast China, *Atmos. Chem. Phys.*, 24, 9869–9883,
591   2024.

592 Chiappini, L., Verlhac, S., Aujay, R., Maenhaut, W., Putaud, J. P., Sciare, J., Jaffrezo, J. L., Liousse,
593   C., Galy-Lacaux, C., Alleman, L. Y., Panteliadis, P., Leoz, E., and Favez, O.: Clues for a
594   standardised thermal-optical protocol for the assessment of organic and elemental carbon
595   within ambient air particulate matter, *Atmos. Meas. Tech.*, 7, 1649–1661, 2014

596 Collaud Coen, M., Weingartner, E., Apituley, A., Ceburnis, D., Fierz-Schmidhauser, R., Flentje, H.,
597   Henzing, J. S., Jennings, S. G., Moerman, M., Petzold, A., Schmid, O., and Baltensperger, U.:
598   Minimizing light absorption measurement artifacts of the Aethalometer: evaluation of five
599   correction algorithms, *Atmos. Meas. Tech.*, 3, 457–474, 2010.

Costa, V., Bacco, D., Castellazzi, S., Ricciardelli, I., Vecchietti, R., Zigola, C., and Pietrogrande, M. C.: Characteristics of carbonaceous aerosols in Emilia-Romagna (Northern Italy) based on two fall/winter field campaigns, *Atmos. Res.*, 167, 100–107, 2016.

Dao, X., Lin, Y. C., Cao, F., Di, S. Y., Hong, Y. H., Xing, G. H., Li, J. J., Fu, P. Q., and Zhang, Y. L.: Introduction to the national aerosol chemical composition monitoring network of China: objectives, current status, and outlook, *Bull. Am. Meteorol. Soc.*, 100, ES337–ES351, 2019.

Eckhardt, S., Pisso, I., Evangeliou, N., Zwaaftink, C. G., Plach, A., McConnell, J. R., Sigl, M., Ruppel, M., Zdanowicz, C., Lim, S., Chellman, N., Opel, T., Meyer, H., Steffensen, J. P., Schwikowski, M., and Stohl, A.: Revised historical Northern Hemisphere black carbon emissions based on inverse modeling of ice core records, *Nat. Commun.*, 14, 271, 2023.

Fuzzi, S., Baltensperger, U., Carslaw, K., Decesari, S., van der Gon, H. D., Facchini, M. C., Fowler, D., Koren, I., Langford, B., Lohmann, U., Nemitz, E., Pandis, S., Riipinen, I., Rudich, Y., Schaap, M., Slowik, J. G., Spracklen, D. V., Vignati, E., Wild, M., Williams, M., and Gilardoni, S.: Particulate matter, air quality and climate: lessons learned and future needs, *Atmos. Chem. Phys.*, 15, 8217–8299, 2015.

Garofalo, L. A., Pothier, M. A., Levin, E. J. T., Campos, T., Kreidenweis, S. M., and Farmer, D. K.: Emission and evolution of submicron organic aerosol in smoke from wildfires in the Western United States, *ACS Earth Space Chem.*, 3, 1237–1247, 2019.

Gao, C. Y., Heald, C. L., Katich, J. M., Luo, G., and Yu, F. Q.: Remote aerosol simulated during the Atmospheric Tomography (ATom) campaign and implications for aerosol lifetime, *J. Geophys. Res. Atmos.*, 127, e2022JD036524, 2022.

Gao, S., Hegg, D. A., Hobbs, P. V., Kirchstetter, T. W., Magi, B. I., and Sadilek, M.: Water-soluble organic components in aerosols associated with savanna fires in southern Africa: identification, evolution, and distribution, *J. Geophys. Res.*, 108, 8491, 2003.

Giannoni, M., Calzolai, G., Chiari,M., Cincinelli, A., Lucarelli, F., Martellini, T., and Nava, S.: A comparison between thermal-optical transmittance elemental carbon measured by different protocols in PM$_{2.5}$ samples, *Sci. Total Environ.*, 571, 195–205, 2016.

Gkatzelis, G. I., Coggon, M. M., Stockwell, C. E., Hornbrook, R. S., Allen, H., Apel, E. C., Bela, M. M., Blake, D. R., Bourgeois, I., Brown, S. S., Campuzano-Jost, P., St. Clair, J. M., Crawford, J. H., Crounse, J. D., Day, D. A., DiGangi, J. P., Diskin, G. S., Fried, A., Gilman, J. B., Guo, H., Hair, J. W., Halliday, H. S., Hanisco, T. F., Hannun, R., Hills, A., Huey, L. G., Jimenez, J. L., Katich, J. M., Lamplugh, A., Lee, Y. R., Liao, J., Lindaas, J., McKeen, S. A., Mikoviny, T., Nault, B. A., Neuman, J. A., Nowak, J. B., Pagonis, D., Peischl, J., Perring, A. E., Piel, F., Rickly, P. S., Robinson, M. A., Rollins, A. W., Ryerson, T. B., Schueneman, M. K., Schwantes, R. H., Schwarz, J. P., Sekimoto, K., Selimovic, V., Shingler, T., Tanner, D. J., Tomsche, L., Vasquez, K. T., Veres, P. R., Washenfelder, R., Weibring, P., Wennberg, P. O., Wisthaler, A., Wolfe, G. M., Womack, C. C., Xu, L., Ball, K., Yokelson, R. J., and Warneke, C.: Parameterizations of US wildfire and prescribed fire emission ratios and emission factors based on FIREX-AQ aircraft measurements, *Atmos. Chem. Phys.*, 24, 929–956, 2024.

Hand, J. L., Prenni, A. J., Raffuse, S. M., Hyslop, N. P., Malm, W. C., and Schichtel, B. A.: Spatial and seasonal variability of remote and urban speciated fine particulate matter in the United States, *J. Geophys. Res. Atmos.*, 129, e2024JD042579, 2024

Hecobian, A., Zhang, X., Zheng, M., Frank, N., Edgerton, E. S., and Weber, R. J.: Water-soluble organic aerosol material and the light-absorption characteristics of aqueous extracts measured over the Southeastern United States, *Atmos. Chem. Phys.*, 10, 5965–5977, 2010.

Hu, Z. F., Kang, S. C., Xu, J. Z., Zhang, C., Li, X. F., Yan, F. P., Zhang, Y. L., Chen, P. F., and Li, C. L.: Significant overestimation of black carbon concentration caused by high organic carbon in aerosols of the Tibetan Plateau, *Atmos. Environ.*, 294, 119486, 2023.

Knox, A., Evans, G. J., Brook, J. R., Yao, X., Jeong, C. H., Godri, K. J., Sabaliauskas, K., and Slowik, J. G.: Mass absorption cross-section of ambient black carbon aerosol in relation to chemical age, *Aerosol Sci. Technol.*, 43, 522–532, 2009.

Laborde, M., Schnaiter, M., Linke, C., Saathoff, H., Naumann, K. H., Möhler, O., Berlenz, S., Wagner, U., Taylor, J. W., Liu, D., Flynn, M., Allan, J. D., Coe, H., Heimerl, K., Dahlkötter, F., Weinzierl, B., Wollny, A. G., Zanatta, M., Cozic, J., Laj, P., Hitzenberger, R., Schwarz, J. P., and Gysel, M.: Single Particle Soot Photometer intercomparison at the AIDA chamber, *Atmos.*

Meas. Tech., 5, 3077–3097, 2012.

Lack, D. A., Moosmüller, H., McMeeking, G. R., Chakrabarty, R. K., and Baumgardner, D.: Characterizing elemental, equivalent black, and refractory black carbon aerosol particles: a review of techniques, their limitations and uncertainties, *Anal. Bioanal. Chem.*, 406, 99–122, 2014.

Lappi, M. K., and Ristimäki, J. M.: Evaluation of thermal optical analysis method of elemental carbon for marine fuel exhaust, *J. Air Waste Manage. Assoc.*, 67, 1298–1318, 2017.

Li, H. Y., Lamb, K. D., Schwarz, J. P., Selimovic, V., Yokelson, R. J., McMeeking, G. R., and May, A. A.: Inter-comparison of black carbon measurement methods for simulated open biomass burning emissions, *Atmos. Environ.*, 206, 156–169, 2019.

Li, J., Carlson, B. E., Yung, Y. L., Lv, D. R., Hansen, J., Penner, J. E., Liao, H., Ramaswamy, V., Kahn, R. A., Zhang, P., Dubovik, O., Ding, A. J., Lacis, A. A., Zhang, L., and Dong, Y. M.: Scattering and absorbing aerosols in the climate system, *Nat. Rev. Earth Environ.*, 3, 363–379, 2022.

Liu J. M., Du Z. Y., Liang L. L., Yu Q. Q., Shen G. F., Ma Y. L., Zheng M., Cheng Y., and He K. B.: Uncertainties in thermal-optical measurements of black carbon: insights from source and ambient samples, *Sci. Total Environ.*, 656, 239–249, 2019.

Liu, J. M., Wang, P. F., Zhang, H. L., Du, Z. Y., Zheng, B., Yu, Q. Q., Zheng, G. J., Ma, Y. L., Zheng, M., Cheng, Y., Zhang, Q., and He, K. B.: Integration of field observation and air quality modeling to characterize Beijing aerosol in different seasons, *Chemosphere*, 242, 125195, 2020.

Liu, S. G., Geng, G. N., Xiao, Q. Y., Zheng, Y. X., Liu, X. D., Cheng, J., and Zhang, Q.: Tracking daily concentrations of $PM_{2.5}$ chemical composition in China since 2000, *Environ. Sci. Technol.*, 56, 16517–16527, 2022.

Liu, X. X., Zhang, Y., Huey, L. G., Yokelson, R. J., Wang, Y., Jimenez, J. L., Campuzano-Jost, P., Beyersdorf, A. J., Blake, D. R., Choi, Y., St Clair, J. M., Crounse, J. D., Day, D. A., Diskin, G. S., Fried, A., Hall, S. R., Hanisco, T. F., King, L. E., Meinardi, S., Mikoviny, T., Palm, B. B.,

Peischl, J., Perring, A. E., Pollack, I. B., Ryerson, T. B., Sachse, G., Schwarz, J. P., Simpson, I. J., Tanner, D. J., Thornhill, K. L., Ullmann, K., Weber, R. J., Wennberg, P. O., Wisthaler, A., Wolfe, G. M., and Ziemba, L. D.: Agricultural fires in the southeastern U.S. during SEAC[4]RS: Emissions of trace gases and particles and evolution of ozone, reactive nitrogen, and organic aerosol, *J. Geophys. Res. Atmos.*, 121, 7383–7414, 2016.

Petzold, A., Ogren, J. A., Fiebig, M., Laj, P., Li, S. M., Baltensperger, U., Holzer-Popp, T., Kinne, S., Pappalardo, G., Sugimoto, N., Wehrli, C., Wiedensohler, A., and Zhang, X. Y.: Recommendations for reporting "black carbon" measurements, *Atmos. Chem. Phys.*, 13, 8365–8379, 2013.

Petzold, A., Schloesser, H., Sheridan, P. J., Arnott, W. P., Ogren, J. A., and Virkkula, A.: Evaluation of multiangle absorption photometry for measuring aerosol light absorption, *Aerosol Sci. Technol.*, 39, 40–51, 2005.

Philip, S., Martin, R., van Donkelaar, A., Lo, J. W. H., Wang, Y. X., Chen, D., Zhang, L., Kasibhatla, P. S., Wang, S. W., Zhang, Q., Lu, Z., Streets, D. G., Bittman, S., and MacDonald, D. J.: Global chemical composition of ambient fine particulate matter for exposure assessment, *Environ. Sci. Technol.*, 48, 13060–13068, 2014.

Piazzalunga, A., Bernardoni, V., Fermo, P., Valli, G., and Vecchi, R.: Technical note: On the effect of water-soluble compounds removal on EC quantification by TOT analysis in urban aerosol samples, *Atmos. Chem. Phys.*, 11, 10193–10203, 2011.

Pileci, R. E., Modini, R. L., Bertò, M., Yuan, J., Corbin, J. C., Marinoni, A., Henzing, B., Moerman, M. M., Putaud, J. P., Spindler, G., Wehner, B., Müller, T., Tuch, T., Trentini, A., Zanatta, M., Baltensperger, U., and Gysel-Beer, M.: Comparison of co-located refractory black carbon (rBC) and elemental carbon (EC) mass concentration measurements during field campaigns at several European sites, *Atmos. Meas. Tech.*, 14, 1379–1403, 2021.

Pöschl, U.: Atmospheric aerosols: composition, transformation, climate and health effects, *Angew. Chem. Int. Ed.*, 44, 7520–7540, 2005.

Putaud, J. P., Van Dingenen, R., Alastuey, A., Bauer, H., Birmili, W., Cyrys, J., Flentje, H., Fuzzi,

S., Gehrig, R., Hansson, H. C., Harrison, R. M., Herrmann, H., Hitzenberger, R., Hüglin, C., Jones, A. M., Kasper-Giebl, A., Kiss, G., Kousa, A., Kuhlbusch, T. A. J., Löschau, G., Maenhaut, W., Molnar, A., Moreno, T., Pekkanen, J., Perrino, C., Pitz, M., Puxbaum, H., Querol, X., Rodriguez, S., Salma, I., Schwarz, J., Smolik, J., Schneider, J., Spindler, G., ten Brink, H., Tursic, J., Viana, M., Wiedensohler, A., and Raes, F.: A European aerosol phenomenology-3: Physical and chemical characteristics of particulate matter from 60 rural, urban, and kerbside sites across Europe, *Atmos. Environ.*, 44, 1308–1320, 2020.

Qin, Y. M., Tan, H. B., Li, Y. J., Li, Z. J., Schurman, M. I., Liu, L., Wu, C., and Chan, C. K.: Chemical characteristics of brown carbon in atmospheric particles at a suburban site near Guangzhou, China, *Atmos. Chem. Phys.*, 18, 16409–16418, 2018.

Samset, B. H., Myhre, G., Herber, A., Kondo, Y., Li, S. M., Moteki, N., Koike, M., Oshima, N., Schwarz, J. P., Balkanski, Y., Bauer, S. E., Bellouin, N., Berntsen, T. K., Bian, H., Chin, M., Diehl, T., Easter, R. C., Ghan, S. J., Iversen, T., Kirkevåg, A., Lamarque, J. F., Lin, G., Liu, X., Penner, J. E., Schulz, M., Seland, Ø., Skeie, R. B., Stier, P., Takemura, T., Tsigaridis, K., and Zhang, K.: Modelled black carbon radiative forcing and atmospheric lifetime in AeroCom Phase II constrained by aircraft observations, *Atmos. Chem. Phys.*, 14, 12465–12477, 2014.

Shen, G. F., Chen, Y. C., Wei, S. Y., Fu, X. F., Zhu, Y., and Tao, S.: Mass absorption efficiency of elemental carbon for source samples from residential biomass and coal combustions, *Atmos. Environ.*, 79, 79–84, 2013.

State Council: Circular on Further Promoting the Pollution Prevention and Control Battle, available at: https://www.gov.cn/zhengce/2021-11/07/content_5649656.htm, 2021.

Subramanian, R., Khlystov, A. Y., and Robinson, A. L.: Effect of peak inert-mode temperature on elemental carbon measured using thermal-optical analysis, *Aerosol Sci. Technol.*, 40, 763–780, 2006.

Sullivan, A. P., Guo, H., Schroder, J. C., Campuzano-Jost, P., Jimenez, J. L., Campos, T., Shah, V., Jaeglé, L., Lee, B. H., Lopez-Hilfiker, F. D., Thornton, J. A., Brown, S. S., and Weber, R. J.: Biomass burning markers and residential burning in the WINTER aircraft campaign, *J. Geophys. Res. Atmos.*, 124, 1846–1861, 2019.

737 Tinorua, S., Denjean, C., Nabat, P., Pont, V., Arnaud, M., Bourrianne, T., Dias Alves, M., and

738   Gardrat, E.: A 2-year intercomparison of three methods for measuring black carbon

739   concentration at a high-altitude research station in Europe, *Atmos. Meas. Tech.*, 17, 3897–3915,

740   2024.

741 von Schneidemesser, E., Monks, P. S., Allan, J. D., Bruhwiler, L., Forster, P., Fowler, D., Lauer, A.,

742   Morgan, W. T., Paasonen, P., Righi, M., Sindelarova, K., and Sutton, M. A.: Chemistry and the

743   linkages between air quality and climate change, *Chem. Rev.*, 115, 3856–3897, 2015.

744 Wang, G. H., Cheng, C. L., Huang, Y., Tao, J., Ren, Y. Q., Wu, F., Meng, J. J., Li, J. J., Cheng, Y. T.,

745   Cao, J. J., Liu, S. X., Zhang, T., Zhang, R., and Chen, Y. B.: Evolution of aerosol chemistry in

746   Xi'an, inland China, during the dust storm period of 2013 – Part 1: Sources, chemical forms

747   and formation mechanisms of nitrate and sulfate, *Atmos. Chem. Phys.*, 14, 11571–11585,

748   2014a.

749 Wang, R., Tao, S., Balkanski, Y., Ciais, P., Boucher, O., Liu, J. F., Piao, S. L., Shen, H. Z., Vuolo,

750   M. R., Valari, M., Chen, H., Chen, Y. C., Cozic, A., Huang, Y., Li, B. G., Li, W., Shen, G. F.,

751   Wang, B., and Zhang, Y. Y.: Exposure to ambient black carbon derived from a unique inventory

752   and high-resolution model, *Proc. Natl. Acad. Sci. U. S. A.*, 111, 2459–2463, 2014b.

753 Wang, X., Heald, C. L., Liu, J. M., Weber, R. J., Campuzano-Jost, P., Jimenez, J. L., Schwarz, J. P.,

754   and Perring, A. E.: Exploring the observational constraints on the simulation of brown carbon,

755   *Atmos. Chem. Phys.*, 18, 635–653, 2018.

756 Wei, J., Li, Z. Q., Lyapustin, A., Wang, J., Dubovik, O., Schwartz, J., Sun, L., Li, C., Liu, S., and

757   Zhu, T.: First close insight into global daily gapless 1 km $PM_{2.5}$ pollution, variability, and health

758   impact, *Nat. Commun.*, 14, 8349, 2023.

759 Xiao, Q. Y., Geng, G. N., Xue, T., Liu, S. G., Cai, C. L., He, K. B., and Zhang, Q.: Tracking $PM_{2.5}$

760   and O_3 Pollution and the related health burden in China 2013-2020, *Environ. Sci. Technol.*,

761   56, 6922–6932, 2022.

762 Yang, H., and Yu, J. Z.: Uncertainties in charring correction in the analysis of elemental and organic

763   carbon in atmospheric particles by thermal/optical methods, *Environ. Sci. Technol.*, 36, 5199–

764   5204, 2002.

765   Yu, J. Z., Xu, J. H., and Yang, H.: Charring characteristics of atmospheric organic particulate matter

766   in thermal analysis, *Environ. Sci. Technol.*, 36, 754–761, 2002.

767   Zheng, G. J., Duan, F. K., Su, H., Ma, Y. L., Cheng, Y., Zheng, B., Zhang, Q., Huang, T., Kimoto,

768   T., Chang, D., Pöschl, U., Cheng, Y. F., and He, K. B.: Exploring the severe winter haze in

769   Beijing: the impact of synoptic weather, regional transport and heterogeneous reactions, *Atmos.*

770   *Chem. Phys.*, 15, 2969–2983, 2015.

771   Zhong, Q. R., Schutgens, N., van der Werf, G. R., Takemura, T., van Noije, T., Mielonen, T., Checa-

772   Garcia, R., Lohmann, U., Kirkevåg, A., Olivié, D. J. L., Kokkola, H., Matsui, H., Kipling, Z.,

773   Ginoux, P., Le Sager, P., Rémy, S., Bian, H. S., Chin, M., Zhang, K., Bauer, S. E., and Tsigaridis,

774   K.: Threefold reduction of modeled uncertainty in direct radiative effects over biomass burning

775   regions by constraining absorbing aerosols, *Sci. Adv.*, 9, eadi3568, 2023.